Available online at www.sciencedirect.com
SCIENCE DIRECT®
PERGAMON
Continental Shelf Research 22 (2002) 2795–2806
CONTINENTAL SHELF RESEARCH
www.elsevier.com/locate/csr

Modelling sand wave migration in shallow shelf seas

Attila A. Németh*, Suzanne J.M.H. Hulscher, Huib J. de Vriend

Department of Civil Engineering, University of Twente, P.O. Box 217, 7500 Enschede, AE, The Netherlands

Received 29 November 2000; accepted 11 January 2002

Abstract

Sand waves form a prominent regular pattern in the offshore seabed of sandy shallow seas. The positions of sand-wave crests and troughs slowly change in time. Sand waves are usually assumed to migrate in the direction of the residual current. This paper considers the physical mechanisms that may cause sand waves to migrate and methods to quantify the associated migration rates. We carried out a theoretical study based on the assumption that sand waves evolve as free instabilities of the system. A linear stability analysis was then performed on a 2DV morphological model describing the interaction between the vertically varying water motion and an erodible bed in a shallow sea. Here, we disrupted the basic tidal symmetry by choosing a combination of a steady current (M_0) and a sinusoidal tidal motion (M_2) as the basic flow. We allowed for two different physical mechanisms to generate the steady current: a sea surface wind stress and a pressure gradient. The results show that similar sand waves develop for both flow conditions and that these sand waves migrate slowly in the direction of the residual flow. The rates of migration and wavelengths found in this work agree with theoretical and empirical values reported in the literature.

Keywords: Stability analysis; Sand waves; Migration; Shelf seas; 2 DV

1. Introduction

Large parts of shallow seas, such as the North Sea (Fig. 1), are covered with bed features that are fascinatingly regular. Sand waves form a prominent bed pattern with a crest spacing of about 500 m. Usually, sand waves (also referred to as dunes as stated by Ashley (1990) are observed at a water depth in the order of 30 m and their heights can reach up to several metres. This means that the relative sand-wave height can be significant. The crests are often assumed to be perpendicular to the principal current (Johnson et al., 1981; Langhorne, 1981; Tobias, 1989). Based on a theoretical analysis, Hulscher (1996) arrived at the conclusion that sand-wave crests may deviate up to 10° anti-clockwise from the direction perpendicular to the principal current.

Observations indicate that these sand waves are dynamic (Maren, 1998; Lanckneus and De Moor, 1991; Allen, 1980) and can migrate with speeds of up to several metres per year. Knowing the spatial and temporal intervals of bed changes will enhance the overall safety of an area (Németh, in preparation):

- The North Sea, for instance, contains hundreds of kilometres of pipelines and cables. A migrating sand-wave can uncover cables and

*Corresponding author.
E-mail address: a.a.nemeth@ctw.utwente.nl (A.A. Németh).

0278-4343/02/$ - see front matter
PII: S0278-4343(02)00127-9

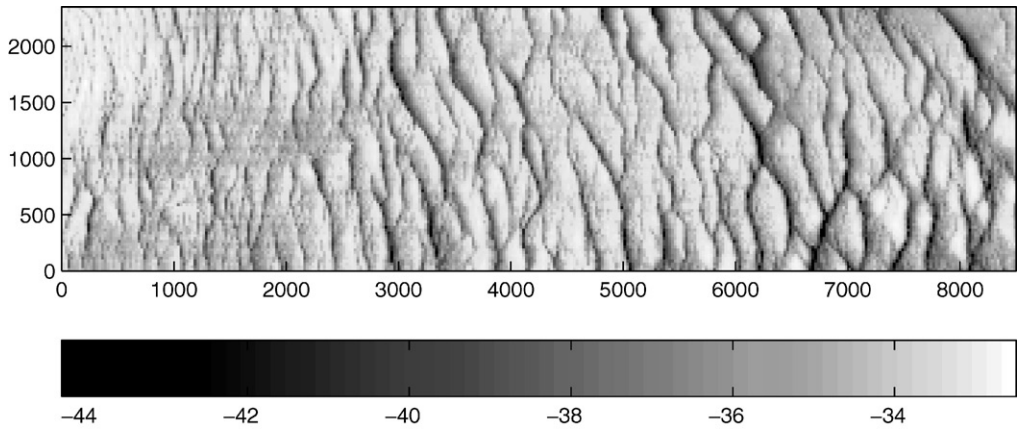

Fig. 1. Bathymetry measurements made in the North Sea near the Eurogeul, with horizontal coordinates specified in metres and a colorbar denoting the sea bed level below mean sea level (in metres). (Courtesy Rijkswaterstaat, North Sea Directorate; details on measurements and analysis are given in Knaapen et al. (2001).)

make them susceptible to damage. Furthermore, free spans can develop, which can lead to bending, vibration, buckling or even breaking of pipelines (Whitehouse et al., 2000).

- Migrating sand waves can also cover mines and chemical waste, which consequently may lie hidden within the seafloor, to become exposed in the future.

Sand-wave migration has been studied in situ by e.g. Lanckneus and De Moor (1991) and Terwindt (1971). The current method for quantifying migration has serious limitations, as data tend to be inaccurate (especially older data). Furthermore, often only the crests are considered, which ignores the major part of the available information. Building long-term data sets and developing objective and accurate methods to process this data will take a considerable amount of time and effort.

To determine sand-wave migration in the field, we need bathymetric data on an annual basis and an accurate positioning method, which enables absolute interrelation of the positioning of bathymetric data in the horizontal domain. The latter is an important limiting factor. In recent years, the location accuracy has greatly improved by the use of GPS. Yet, the yearly migration rates are still of the same order of magnitude as the horizontal positioning error. We are working on an objective and accurate method, based on bathymetry data over a number of years, to determine actual migration rates. This will enable us to compare the model results with actual data. This is crucial for understanding sand-wave migration and the processes involved. More specifically, it will reveal whether the rather simple model discussed within this paper is sufficient, or whether extensions are needed in order to describe sand-wave migration.

Sand-wave migration has been modelled in the past as a direct extension of bedform dynamics in rivers (Fredsøe and Deigaard, 1992). However, the residual current in a tidal environment is much smaller than the steady currents found in rivers. Therefore, the migration velocities of tidal sand waves are one to two orders of magnitude smaller than the velocities attained by dunes in rivers Allen, 1980. Fredsøe and Deigaard (1992) describe the behaviour of finite-amplitude dunes under a steady current. They assume the time-dependency of the flow to be negligible when modelling sand waves in a tidal environment.

Huthnance (1982) was the first to look at a system consisting of depth-averaged tidal flow and an erodible seabed. Within this framework, one can investigate whether certain regular patterns develop as free instabilities of the system. Unstable modes comparable to tidal sandbanks were found, whereas smaller modes corresponding to sand waves were not initiated. Hulscher (1996) extended

this work by using a model allowing for vertical circulations and found formation of sand waves due to a basic tidal motion that was horizontally uniform and symmetrical in time. Hulscher (1996) showed that net convergence of sand can occur at the top of the sand waves over an entire tidal cycle (see also Gerkema, 2000; Komarova and Hulscher, 2000). In these models, sand waves do not migrate. Hulscher and Van den Brink (2001) showed the predictive ability of their model for sand-wave occurrence. Blondeaux et al. (1999) introduced forcing due to surface waves on top of the tidal motion. These wind waves accomplish a net transport of energy and the authors found migration of sand waves. However, the numerical treatment left many questions about the specific mechanisms behind migration unanswered. Komarova and Newell (2000) extended a linear analysis (Komarova and Hulscher, 2000) into the weakly non-linear regime to investigate the behaviour of finite-amplitude sand waves. The latter model does not include migration, either.

We can conclude that the cause and migration of sand waves are not fully understood yet. This paper is based upon a model in which sand-wave migration by a residual flow is allowed. The paper tests the hypothesis that tidal movement is responsible for the evolution of sand waves and that steady currents cause these features to migrate. It also discusses prediction of migration rates.

In Section 2 we present a scaling method appropriate for sand waves. Furthermore, a non-dimensional idealised model is presented. It is based on the two-dimensional vertical shallow water equations combined with a simple sediment transport equation, describing bed load transport. The morphological changes are calculated over a longer time scale than the water movement. This makes it possible to average the bottom evolution over the tidal period. In Section 3 we show the results of a linear stability analysis. We start with a basic state, which consists of a steady current, on top of symmetrical tidal movement (M_2). This steady current is either induced by a wind stress applied at the sea surface or by a pressure gradient. The initial behaviour of the system is then investigated by looking at the feedback of small-amplitude sand waves. Also, a sensitivity analysis is performed on this linear stability analysis. In Section 4 we will discuss the results. The fifth and final section contains the conclusions and generalisations of the results.

2. Description of the analytical model

The model presented in this paper is based on analytical models constructed by Hulscher (1996), Gerkema (2000) and Komarova and Hulscher (2000). The Coriolis force only slightly affects sand waves. The behaviour of sand waves can therefore be described with the help of the two-dimensional vertical (2DV) shallow water equations.

2.1. Scaling

Before a particular choice is made concerning the method of scaling, we will first summarise the variables and parameters that are assumed to play an important role in sand-wave behaviour (Table 1). The values chosen in Table 1 represent a typical North Sea location. Next, typical scaling methods used in the past are summarised in Table 2. The last column of Table 2 shows the scaling method used in this paper. The symbols g and A_v indicate, respectively, the acceleration due to gravity and the constant vertical eddy viscosity. Time is represented by t and is scaled with the tidal frequency represented by σ. This is because tidal movement is assumed to be the main forcing mechanism of the large-scale bed forms. The velocities in the x- and z-directions are u, respectively, w. The horizontal velocity (x) is

Table 1
Scaling parameters and variables

Scaling parameters	Symbol	Default value	Dimension
Tidal frequency	σ	1.4×10^{-4}	s^{-1}
Maximum current velocity	U	$1\ m\ s^{-1}$	$m\ s^{-1}$
Average water depth	H	30	m
Stokes layer thickness	δ	12	m
Kinematic viscosity	A_v	1×10^{-2}	$m^2\ s^{-1}$
Gravitational acceleration	g	9.8	$m\ s^{-2}$
Morphological length scale	ℓ_m	500	m

Table 2
Overview scaling methods (blank means not discussed or not appropriate for comparison)

Variable	Hulscher (1996)	Gerkema (2000)	Komarova and Hulscher (2000)	This paper
u/u_*	U	U	U	U
w/w_*	σH	$UH\hat{k}$	U	$\frac{1}{10}U$
x/x_*	$U\sigma^{-1}$	$\hat{k}^{-1}$	δ	10δ
z/z_*	H	H	δ	δ
t/t_*	σ^{-1}	σ^{-1}	σ^{-1}	σ^{-1}
ζ/ζ_*	$UL\sigma g^{-1}$	.	$U^2 g^{-1}$	$UL\sigma g^{-1}$
τ_b/τ_{b*}	$UH\sigma$	.	$A_v U\delta^{-1}$	$A_v U\delta^{-1}$
h/h_*	H	H	H	H
p/p_*	.	.	$\rho\sigma^2\delta^2$	.

The asterisk $*$ denotes a non-dimensional quantity.

scaled with the tidal velocity amplitude (U). The vertical co-ordinate is denoted by z and h represents the amplitude of the bottom perturbation. They are both scaled with the Stokes depth (δ). The thickness of the tidal boundary layer is related to δ defined by

$$\delta = \sqrt{\frac{2A_v}{\sigma}}. \tag{1}$$

The vertical velocity (w) and the horizontal length scale (x) is scaled with the Stokes depth. They are furthermore divided and multiplied by a factor 10, respectively, so as to make it possible to scale the variables with physically relevant scales, combined with a correct order of magnitude. This value is obtained by looking at the balance between the shear stress and the slope term in the sediment transport formula (Komarova and Hulscher, 2000). Gerkema (2000) uses a wavenumber defined by

$$\tilde{k} = \frac{2\pi}{\text{length sand wave}}. \tag{2}$$

The water level ($z = \zeta$) is scaled with the length over which the tidal wave varies (L). τ_b is the bottom shear stress and scaled analogous to the definition of shear stress gives

$$\tau_b = \left.\frac{\partial u}{\partial z}\right|_{z=-1+h}. \tag{3}$$

2.2. Flow model

Starting from the 2DV shallow water equations, neglecting the horizontal viscosity and using the scaling presented in Table 2, last column (for convenience $*$ is dropped) we arrive at

$$\frac{\partial u}{\partial t} + Ru\frac{\partial u}{\partial x} + Rw\frac{\partial u}{\partial z} = -R\frac{L\sigma}{U}\frac{\partial \zeta}{\partial x} + \frac{\partial}{\partial z}\left(E_v\frac{\partial u}{\partial z}\right), \tag{4}$$

$$\frac{\partial u}{\partial x} + \frac{\partial w}{\partial z} = 0, \tag{5}$$

with

$$E_v = \frac{A_v}{\delta^2\sigma}, \quad R = \frac{U}{10\delta\sigma}. \tag{6}$$

E_v can be seen as a measure for the influence of the viscosity on the water movement (by definition the tidal movement) in the water column. R is a function of the square root of the Reynolds number (Fig. 2).

2.3. Boundary conditions and assumptions

The boundaries in the horizontal plane are located infinitely far away. The boundary conditions at the water surface ($z = \zeta$) are defined as follows:

$$\frac{L\sigma^2 10}{g}\frac{\partial \zeta}{\partial t} + \frac{UL\sigma}{g\delta}u\frac{\partial \zeta}{\partial x} = w, \tag{7}$$

$$\frac{\partial u}{\partial z} = \hat{\tau_w}, \tag{8}$$

with

$$\hat{\tau_w} = \frac{\delta}{UA_v}\tau_w, \tag{9}$$

in which τ_w describes the wind induced stress at the sea surface. The horizontal flow components at the bottom are described with the help of a partial slip

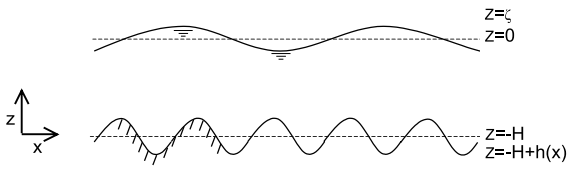

Fig. 2. Definition sketch of the model geometry.

condition (S is the resistance parameter controlling the resistance at the seabed). Models, using a z-independent eddy viscosity formulation and a no-slip condition tend to overestimate the bottom shear stress. The shear stress determines directly the amount of sediment transported. Therefore, a partial-slip model with a finite value of the resistance parameter S is needed in order to produce realistic results. The vertical velocity component at the bed ($z=-1+h$) is described by the kinematic condition:

$$\frac{\partial h}{\partial t}+u\frac{\partial h}{\partial x}=w, \tag{10}$$

$$E_v\frac{\partial u}{\partial z}=\hat{S}u, \tag{11}$$

with

$$\hat{S}=\frac{S}{\sigma\delta}. \tag{12}$$

2.4. Sediment transport and seabed behaviour

The sediment transport model only describes bed load transport. This mode of transport is assumed to be dominant in offshore tidal regimes. As the flow velocities in the vertical direction are being calculated explicitly, bed load transport can be modelled here as a direct function of the bottom shear stress. The following general bed load formula is used (Komarova and Hulscher, 2000):

$$S_b=\alpha\left(\frac{A_vU}{\sigma}\right)^{1+b}|\tau_b|^b\left[\tau_b-\hat{\lambda}\frac{\partial h}{\partial x}\right]. \tag{13}$$

S_b is the volumetric sediment transport. The power of transport, represented by b is set at $1/2$. The proportionality constant α can be computed from Van Rijn (1993). It is set at a value of about $0.3\ \mathrm{m}^{-2}$ s. The scale factor for the bed slope mechanism is λ. It takes into account that sand is transported more easily downward than upward. The default value is set at 0.0085 in this study (Komarova and Hulscher, 2000). The effects of the critical shear stress on the slope effects are incorporated herein.

The net inflow of sediment is assumed to be zero. This results in the following sediment balance, which couples the flow model (4)–(12) with the sediment transport model (13):

$$\frac{\partial h}{\partial T_m}=-\frac{\partial}{\partial x}\left(|\tau_b|^b\left[\tau_b-\hat{\lambda}\frac{\partial h}{\partial x}\right]\right), \tag{14}$$

in which

$$\hat{\lambda}=\frac{\delta}{10A_vU}\lambda,\quad T_m=\hat{\alpha}t,$$

$$\hat{\alpha}=\frac{\alpha}{10\delta^2\sigma}\left(\frac{A_vU}{\delta}\right)^{1+b}\equiv\frac{1}{\sigma T_{long}}. \tag{15}$$

The bed level will hardly vary on a tidal time scale. The behaviour of the bed is therefore evaluated on a larger time-scale by considering tidally averaged values for the sediment transport.

3. Linear stability analysis

The solution of the problem can formally be presented by the vector $\psi=(u,w,\zeta,h)$. The sand-wave amplitude to water depth ratio is denoted by γ. Starting from an exact solution of the problem, a certain basic state ψ_0 can be perturbed by a small amplitude ($\gamma\ll1$) perturbation. The solution can be expanded as follows:

$$\psi=\psi_0+\gamma\psi_1+\gamma^2\psi_2+\gamma^3\psi_3+\cdots. \tag{16}$$

For $\gamma<1$ and $\|\psi_i\|=\mathcal{O}(1)$ the successive terms decrease in magnitude. This means that the one but largest contribution is fully given by the term ψ_1 being linear in γ. Therefore, the instability of the basic state ψ_0 can be tested by determining the initial behaviour of ψ_1. Amplification of ψ_1 in time implies that the basic state is unstable and decay means stability.

3.1. Basic state

The basic state describes a tidal current together with a steady current over a flat bottom (horizontally uniform flow). The basic vertical velocity turns out to be equal to zero, i.e. $w_0=0$. The horizontal basic flow, u_0, satisfies the following equation:

$$\frac{\partial u_0}{\partial t}=-R\frac{L\sigma}{U}\frac{\partial\zeta_0}{\partial x}+\frac{\partial}{\partial z}\left(E_v\frac{\partial u_0}{\partial z}\right). \tag{17}$$

The boundary condition at the free water surface $z = 0$ is given by

$$\frac{\partial u_0}{\partial x} = \tau_w, \tag{18}$$

and the boundary conditions at the seabed $z = -1$:

$$E_v \frac{\partial u_0}{\partial z} = \hat{S} u_0, \quad w_0 = 0. \tag{19}$$

The velocity in the horizontal direction consists firstly of a periodic part, which represents M_2 tidal motion. The periodic part of the water motion has a depth-averaged amplitude of 1 m s^{-1} (Hulscher, 1996). Secondly, we furthermore disrupt the symmetry by adding a steady current ($u_r(z)$). The basic state can now be formulated as follows:

$$u_0 = \beta u_r(z) + (1 - \beta)\{u_s(z) \sin t + u_c(z) \cos t\}, \tag{20}$$

in which β enables us to vary the ratio of in the steady part and the periodic part, in such a way that the maximum velocity always coincides with the velocity used to scale the system. Two possible types of steady flow component have been investigated. These are (I) a wind driven current and (II) a current induced by a pressure gradient. The vertical structure for each of these cases follows from Eq. (17):

$$\text{I}: u_r = \hat{\tau_w}\left(1 + \frac{E_v}{S} + z\right), \tag{21}$$

$$\text{II}: u_r = P\left(\tfrac{1}{2}z^2 - \frac{E_v}{S} - \tfrac{1}{2}\right), \quad \text{with } P = \frac{L}{10\delta E_v}\zeta. \tag{22}$$

Note that in the wind driven case (I), the shear stress at the bottom is equal to the wind stress at the sea surface. This is only the case if the wind-driven current encounters no obstacles.

3.2. Perturbed state

The stability of the basic state can be tested by determining the initial behaviour of the first-order perturbation. Using Eq. (16) and using the basic state solution Eqs. (17)–(19) gives

$$\frac{\partial u_1}{\partial t} + Ru_0 \frac{\partial u_1}{\partial x} + Rw_1 \frac{\partial u_0}{\partial z} = -R\frac{L\sigma}{U}\frac{\partial \zeta_1}{\partial x} + \frac{\partial}{\partial z}\left(E_v \frac{\partial u_1}{\partial z}\right), \tag{23}$$

$$\frac{\partial u_1}{\partial x} + \frac{\partial w_1}{\partial z} = 0. \tag{24}$$

A Taylor expansion in the small parameter γ enables us to transfer the free surface boundary condition from $z = \zeta$ to $z = 0$ and the bottom boundary condition from $z = -1 + h$ to $z = -1$. The boundary conditions at the free surface are then given by

$$\frac{\partial u_1}{\partial z} = w_1, \tag{25}$$

and at the bottom:

$$\frac{\partial u_1}{\partial z} = \frac{\hat{S}}{E_v} u_1 + h_1 \frac{\hat{S}}{E_v}\frac{\partial u_0}{\partial z} - h_1 \frac{\partial^2 u_0}{\partial z^2}. \tag{26}$$

The unknowns are Fourier transformed as follows with $\psi_1 = (u_1, w_1, \zeta_1, h_1)$:

$$\psi_1 = \int \tilde{\psi}(t) \mathrm{e}^{-\mathrm{i}kx}\, \mathrm{d}k + \text{c.c.}, \tag{27}$$

in which c.c. means complex conjugate and k is the wave number of the wavy bottom perturbation. Harmonic truncation in time is applied. This means that the perturbation is restricted to a finite number of tidal components. In the case of a unidirectional tidal flow, the following truncation will contain the dominant physical processes:

$$\hat{u}_{\text{trunc}}(z, t) = \tilde{h}[\mathrm{i}a_0(z) + a_s(z) \sin t + a_c(z) \cos t], \tag{28}$$

$$\hat{w}_{\text{trunc}}(z, t) = \tilde{h}[c_0(z) + \mathrm{i}c_s(z) \sin t + \mathrm{i}c_c(z) \cos t], \tag{29}$$

$$\hat{\zeta}_{\text{trunc}}(z, t) = \tilde{h}[d_0 + \mathrm{i}d_s \sin t + \mathrm{i}d_c \cos t]. \tag{30}$$

The vertical structure (functions $a_s(z)$, etc.) can now be solved numerically. Subsequently, the shear stress can be calculated and imported into the bottom evolution equation. The evolution of the seabed can best be described by averaging the sediment fluxes over the tidal period, because the seabed will hardly vary on a tidal time scale. The solution for the bottom evolution equation reads:

$$\tilde{h} = h_0 \mathrm{e}^{\omega_r T_m} \cos(kx - \omega_i T_m). \tag{31}$$

This expression represents a progressive wave, the amplitude of which changes in time, starting from the initial value h_0. The complex growth rate ω is

$$\begin{aligned}\omega &= \omega_r + \mathrm{i}\omega_i \\ &= -k(b+1)a_0'(-1)\langle|\tau_{b0}|^b\rangle - \hat{\lambda}k^2\langle|\tau_{b0}|^b\rangle \\ &\quad - \mathrm{i}k(b+1)[a_s'(-1)\langle|\tau_{b0}|^b\sin t\rangle \\ &\quad + a_c'(-1)\langle|\tau_{b0}|^b\cos t\rangle],\end{aligned} \tag{32}$$

in which the brackets denote the tidal average and τ_{b0} the bottom stress of the basic flow. With this equation the initial response of the bed to the introduced perturbation can be investigated.

4. Results

The real part of Eq. (32) (ω_r) represents the dimensionless initial growth rate of the sand waves. If the steady current βu_r equals zero, the water motion is symmetric. In Figs. 3a and b the results are shown for a tidal current with a depth averaged amplitude of 1 m s^{-1} (M_2, $\beta = 0$). The morphological time scale (T_m) is about 6 years (Eq. (15)). This is in line with Hulscher et al. (2000), who investigated data sets and found a time scale of 8 years. As was found from previous research (Gerkema, 2000; Hulscher, 1996; Komarova and Hulscher, 2000; Blondeaux et al., 1999) positive growth rates appear for a range of wave numbers k ($\omega_r > 0$). The wavelength having the largest growth rate is the mode we expect to find in nature. The dimensional wavelength follows from:

$$L_{sandwave} = \frac{20\pi}{k}\sqrt{\frac{2A_v}{\sigma}}. \tag{33}$$

In this case the fastest growing mode has a wave number $k = 1.25$ (see Fig. 3a), which according to Table 2, corresponds with a wavelength of about 600 m. In this case, no migration is found.

The phase speed of the sand waves is described by ω_i/k in which ω_i is the imaginary part of Eq. (32). These phase speeds are due to the asymmetry in the water motion. The magnitude depends on the nature of the steady part (I or II) and on the magnitude of the asymmetry in the water movement. Fig. 3a and b show the results for a depth-averaged residual current of 0.1 m s^{-1} (M_0) superimposed on a tidal current of 0.9 m s^{-1} (M_2) ($\beta = 0.1$).

The fastest growing modes have wavelengths in the order of 700 m in both cases (Fig. 3a). The angular frequency in case of a net current generated by a pressure gradient from that in case of a wind-driven current. The sand waves migrate at a dimensionless rate ω_i/k, in its dimensional form

$$V_{sandwave} = \frac{10\omega_i}{2\pi T_m}\sqrt{\frac{2A_v}{\sigma}}. \tag{34}$$

The pressure gradient (case II) induces larger migration rates than a wind stress (case I). For the

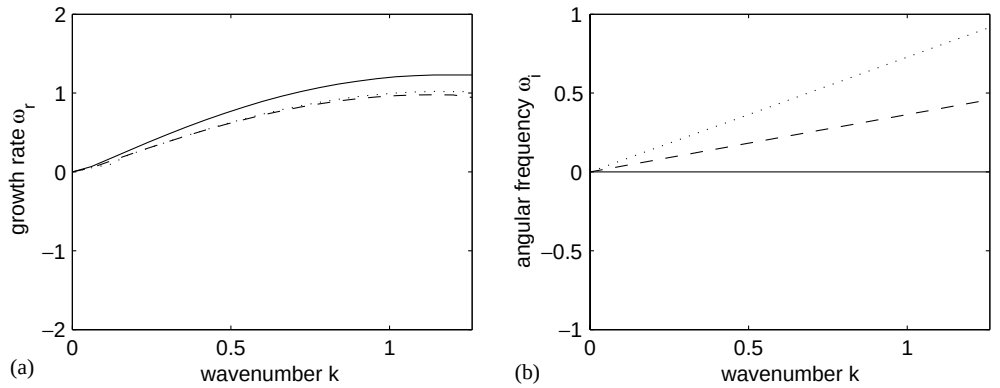

Fig. 3. Growth characteristics as a function of the wave number k: (a) growth rate ω_r and (b) angular frequency ω_i, both for three cases: M_2 (solid), M_2 plus wind (dashed) and M_2 plus pressure gradient (dotted).

fastest growing modes the migration rates for case I become 3 and for case II 10 m yr^{-1}. These are shown in Fig. 3b.

In order to assess the sensitivity to the type of driving force of the net current, we combined the velocity profile of case I with the bed shear stress of case II. The result was a growth and migration rate close to that of case II. This shows that the bed shear stress is the dominant factor in linear sand-wave dynamics. By implication, the parameterisation of the velocity profile is of a lesser importance.

The order of magnitude is similar to values found in the literature (Allen, 1980; Lanckneus and De Moor, 1991; Maren, 1998). It should be noted that inclusion of higher harmonic modes (M_4, M_6, etc.) will give contributions to Eq. (32) which are not taken into account here. However, for most locations the M_0 is assumed to give the largest contribution to the tidal asymmetry, so that it is likely to also play the most important role in sand-wave migration. Further investigation, which incorporate higher harmonics, should test these expectations.

This model is likely to overestimate migration rates. The residual current is time-invariant, i.e. it always has the same strength and orientation. It is necessarily oriented perpendicular to the sand-wave crests, due to the exclusion of the second horizontal dimension. If a different direction is incorporated, the net current responsible for migration, would have been the component perpendicular to the crests (Fig. 4). Furthermore, u_r has to be interpreted as a typical yearly averaged current.[1] In nature, this current will gradually change through time in magnitude and in orientation in time. The latter means that the tidal and the residual current will have different orientations, again. The effective residual current for sand-wave migration will therefore be smaller than the magnitude of the residual current actually observe.

[1] According to Dronkers et al. (1990), the average subsurface residual current in the southern North Sea is directed northward and has a magnitude in the order of 0.05 m s^{-1} (see also Van der Molen, 2000).

5. Sensitivity analysis

Now we perform a sensitivity analysis for the resistance parameter, the viscosity and the slope parameter. For any combination of these parameters, the fastest growing mode can be determined. The analysis is performed for a depth-averaged residual current of 0.1 m s^{-1} (M_0), induced by a pressure gradient (case II), on top of tidal movement of 0.9 m s^{-1} (M_2) ($\beta = 0.1$).

Figs. 5a and b show the wave number of the fastest growing modes and the corresponding growth rate, respectively, both as a function of the dimensionless resistance parameter divided by E_v. If the resistance at the seabed increases, the critical wave number and the growth rate increases (smaller wavelengths are found). The opposite holds for an increase in viscosity. The range on the horizontal axis between 0.03 and 0.08 coincides with wavelengths between 3000 and 500 m. We have to keep in mind that the dimensional wavelength for equal dimensionless wave numbers changes for different values of viscosity. This is due to the use of the Stokes layer thickness instead of the water depth when scaling the spatial coordinates (Table 2). If the viscosity increases, the Stokes layer thickness increases also, thus changing the length scale. Furthermore, the time scale increases with the eddy viscosity (see Eq. (15)). This means that the differences in the actual dimensional growth rates will be smaller, although still present (Fig. 6).

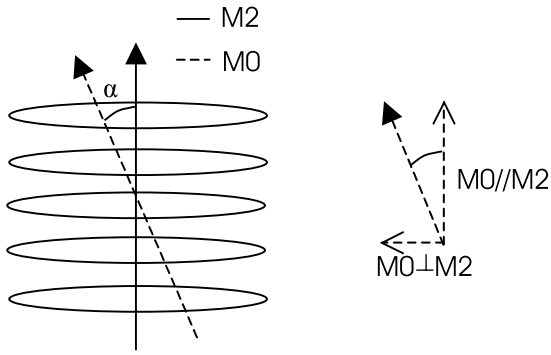

Fig. 4. Orientation residual current with respect to tidal movement.

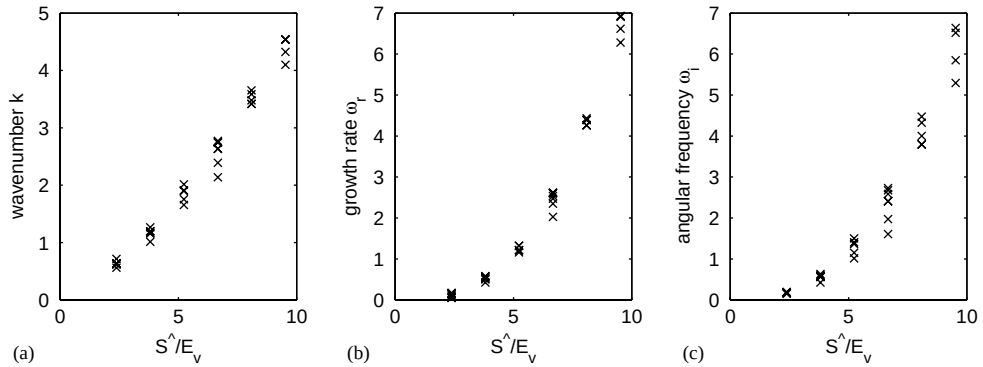

Fig. 5. Properties of the fastest growing modes a function of $\hat{S}/E_v$: (a) wavenumber k, (b) growth rate ω_r and (c) angular frequency ω_i.

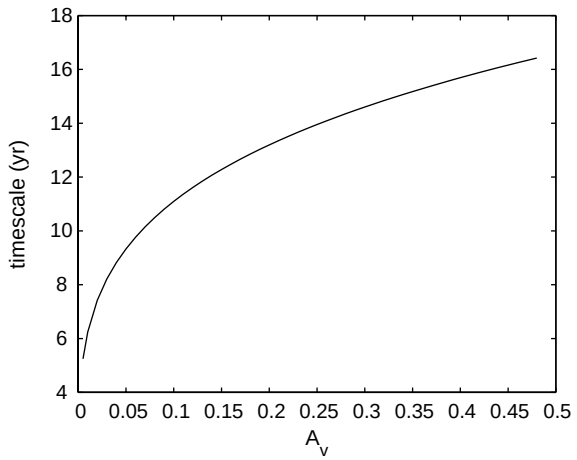

Fig. 6. Time scale as a function of viscosity A_v.

Fig. 5c shows the angular frequency of the fastest growing mode. This quantity becomes smaller for longer wavelengths. If the value of the resistance parameter is increased, the angular frequency will increases too. For the smaller values of the viscosity this relation is stronger. This is due to the fact that for these smaller values of the viscosity the wavelength of the fastest growing mode is much smaller.

If we plot the wavelength against A_v and S we see that if we increase the viscosity or decrease the resistance parameter, the wavelength of the fastest growing mode will increase (Fig. 7a). If we look at the migration rates per year for the same range of A_v and S, we find a very strong dependency on the resistance parameter (Fig. 7b). The slope term does not have a direct effect on the rate of migration, but the slope term does play an important role in determining the fastest growing mode. The slope term dampens the smaller bed forms (see Eq. (14)). Therefore, if we increase this term, the wave number of the fastest growing mode will become smaller. This corresponds with a larger wavelength having a smaller angular frequency. This means that the expected migration rate is indirectly decreased due to a different fastest growing mode.

In addition to the above sensitivity analysis, we have investigated the effect of varying the magnitude of the net current. It appeared that when β is varied, the default values of the resistance parameter and the slope parameter should be reconsidered If the bed resistance is too small, very long bed forms will emerge if the ratio tidal movement/steady current decreases. If we increase the resistance by only a factor two, sand-wave-like bed forms are found again. This can be see from Figs. 8a and b showing the wavenumbers and phase shifts for the fastest growing modes for different values of the resistance parameter with are unstable. A similar sensitivity was found for the slope parameter (λ).

Furthermore, the real part of omega is hardly influenced by the addition of the residual current. The wave number of the fastest growing mode is almost the same as in the case of only symmetrical tidal movement. Gerkema (2000) showed that value for the growth rate and for the wavelength

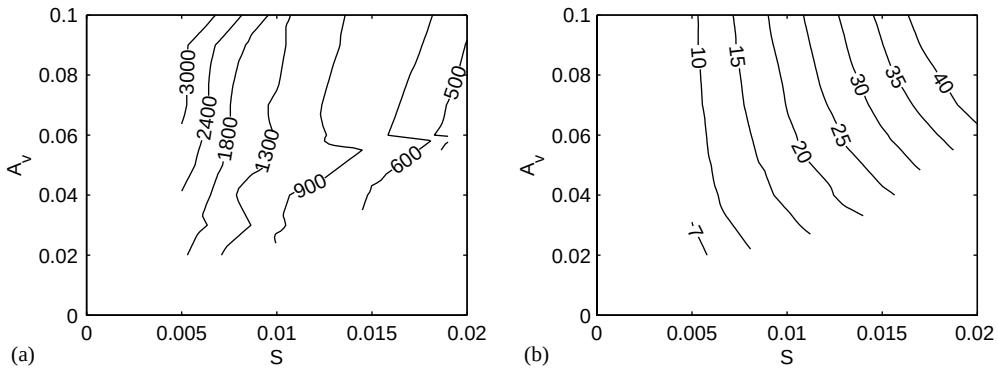

Fig. 7. Properties of the fastest growing mode as a function of S for different values of A_v: (a) Wavelength (m) and (b) migration rate (m yr^{-1}).

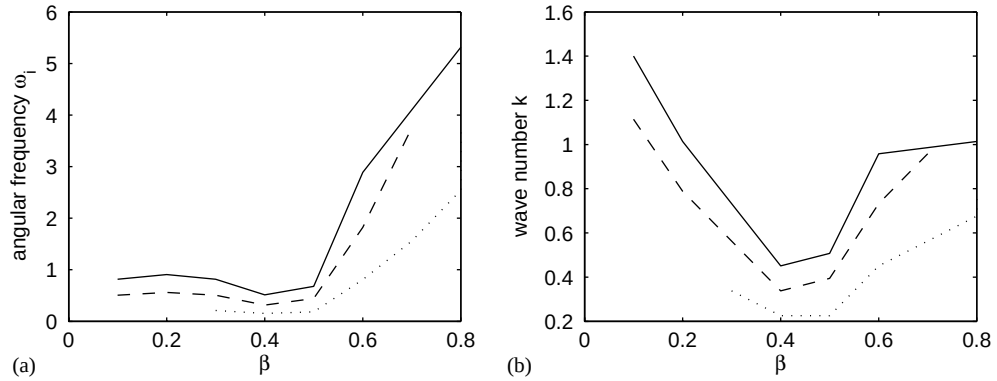

Fig. 8. Properties of the fastest growing mode as a function of β for different values of the resistance parameter: $S = 0.01$ (solid), $S = 0.008$ (dashed) and $S = 0.005$ (dotted): (a) angular frequency ω_i and (b) wavenumber k.

can vary 28 and 13 percent, respectively, due to harmonic truncation. Due to the structure of the problem we expect similar deviations for the model presented in this paper, which do not affect the main conclusions.

In the expression of the imaginary part of omega, the wavenumber can also be found. Since this wavenumber of the fastest growing does not vary a lot due to the inclusion of a residual current, we do not expect a large difference in the migration rate with respect to the dependency on the wavenumber.

6. Conclusions and discussion

The foregoing analysis shows that a steady current inducing an asymmetry in the basic state can cause migration of sand waves. The order of magnitude for the migration rates and wavelengths found (5–10 m yr^{-1} and 600 m, respectively) are in agreement with values reported in the literature. The wavelengths are only slightly influenced by the presence of a steady current superimposed on the M_2 tidal motion.

The steady current can be generated by (I) a wind stress and (II) a pressure gradient causing different magnitudes of the shear stress at the seabed, which in turn causes differences in the migration rate in the order of a factor 3. The predicted wavelength is about the same in either case.

Therefore, tidal currents are the main mechanism responsible for the formation of sand waves in this model. The inclusion of a steady current has only minor effects on the formation process.

Furthermore, the steady current proved to cause sand-wave migration.

Moreover, we found that the asymmetry in the basic bed shear stress is the most important factor in determining the migration of sand waves, the parameterisation of the velocity profile is of lesser importance. This implies that estimates for sand-wave migration rates can be obtained directly from their basic tidal bed shear stress (τ_{b0}) which probably also yields for tidal asymmetries caused by higher harmonics e.g. M_4 (see also Soulsby, 1990) which are not explicitly taken into account here.

We also found a strong dependency of the results, while varying the value of β in Eq. (20), on the value of the resistance and slope parameter (see also Hulscher, 1996; Gerkema, 2000).

Acknowledgements

This work is performed within the EU-sponsored project HUMOR (HUman interaction with large-scale coastal MORphologic evolution; EVK3-CT-2000-00037) and has been co-sponsored by Technology Foundation STW, the applied science division of NWO and the technology programme of the Ministry of Economic Affairs. Furthermore we would like to thank R.M.J. van Damme for his comments.

Appendix A. Solution vertical flow structure

The solution of the linear stability problem describes the flow field as a function of the position in the vertical. The equations describing the perturbed tidal and steady current components are

$$E_v a_0'' = -R\left(k\frac{L\sigma}{U}d_0 + \mathrm{i}ku_r a_0 + \tfrac{1}{2}ku_c - \tfrac{1}{2}c_c u_c' + \tfrac{1}{2}ka_s u_s - \tfrac{1}{2}c_s u_s' + \mathrm{i}c_0 u_r'\right), \quad (A.1)$$

$$E_v a_s'' = -a_c + R\left(k\frac{L\sigma}{U}d_s + c_0 u_s' - \mathrm{i}ka_s u_r + \mathrm{i}c_s u_r' + ka_0 u_s\right), \quad (A.2)$$

$$E_v a_c'' = a_s + R\left(k\frac{L\sigma}{U}d_c + c_0 u_c' - \mathrm{i}ka_c u_r + \mathrm{i}c_c u_r' + ka_0 u_c\right), \quad (A.3)$$

$$c_0' = -ka_0, \quad c_s' = ka_s, \quad c_c' = ka_c. \quad (A.4)$$

Furthermore, the following for the boundary conditions at the free surface are needed:

$$\frac{\partial a_0}{\partial z} = \frac{\partial a_s}{\partial z} = \frac{\partial a_c}{\partial z} = c_0 = c_s = c_c = 0. \quad (A.5)$$

And at the bed:

$$a_0' = \frac{\hat{S}}{E_v}a_0 - \mathrm{i}\frac{\hat{S}}{E_v}u_r'' + \mathrm{i}u_r', \quad (A.6)$$

$$a_s' = \frac{\hat{S}}{E_v}\{a_s + u_s'\} - u_s'', \quad (A.7)$$

$$a_c' = \frac{\hat{S}}{E_v}\{a_c + u_c'\} - u_c'', \quad (A.8)$$

$$c_0 = -\mathrm{i}ku_r, \quad c_s = -ku_s, \quad c_c = -ku_c. \quad (A.9)$$

References

Allen, J.R.L., 1980. Sand wave immobility and the internal master bedding of sand wave deposits. Geological Magazine 117 (5), 347–446.

Ashley, G.M., 1990. Classification of large-scale subaqueous bedforms: a new look at an old problem. Journal of Sedimentary Petrology 60 (1), 160–172.

Blondeaux, P., Brocchini, M., Drago, M., Iovenitti, L., Vittori, G., 1999. Sand waves formation: Preliminary comparison between theoretical predictions and field data. Proceedings of the IAHR Symposium on River Coastal and Estuarine Morphodynamics, Genova, Italy, Vol. 1, pp. 197–206.

Dronkers, J., Van Alphen, J.S.L.J., Borst, J.C., 1990. Suspended sediment transport processes in the Southern North Sea. Coastal and Estuarine Studies 38, 302–320.

Fredsøe, J., Deigaard, R., 1992. Mechanics of coastal sediment transport, Institute of Hydrodynamics and Hydraulic Engineering, Technical University of Denmark, pp. 260–289.

Gerkema, T., 2000. A linear stability analysis of tidally generated sand waves. Journal of Fluid Mechanics 417, 303–322.

Hulscher, S.J.M.H., 1996. Tidal induced large-scale regular bed form patterns in a three-dimensional shallow water model. Journal of Geophysical Research 101 (C9), 20 727–20 744.

Hulscher, S.J.M.H., Van den Brink, G.M., 2001. Comparison between predicted and observed sand waves and sand banks in the North Sea. Journal of Geophysical Research 106 (C5), 9327–9338.

Hulscher, S.J.M.H., Knaapen, M.A.F., Scholl, O., 2000. Regeneration of dredged sandwaves. Proceedings Marine Sandwave Dynamics, Lille, France, pp. 93–95.

Huthnance, J.M., 1982. On one mechanism forming linear sand banks. Estuarine Coastal and Shelf Science 14, 79–99.

Johnson, M.A., Stride, A.H., Belderson, R.H., Kenyon, N.H., 1981. Predicted sand wave formation and decay on a large offshore tidal-current sand-sheet. Special Publications of the International Association of Sediment 5, 247–256.

Knaapen, M.A.F., Hulscher, S.J.M.H., De Vriend, H.J., Stolk, A., 2001. A new type of bedwaves. Geophysical Research Letters 28 (7), 1323–1326.

Komarova, N.L., Hulscher, S.J.M.H., 2000. Linear instability mechanisms for sand wave formation. Journal of Fluid Mechanics 413, 219–246.

Komarova, N.L., Newell, A.C., 2000. Non-linear dynamics of sand banks and sand waves. Journal of Fluid Mechanics 415, 285–321.

Lanckneus, J., De Moor, G., 1991. Present-day evolution of sand waves on a sandy shelf bank. Oceanologica Acta. Proceedings of the International Colloquium on the Environment of Epicontinental Seas, Lille, Vol. sp. No. 11, pp. 123–127.

Langhorne, D.N., 1981. An evaluation of Bagnold's dimensionless coefficient of proportionality using measurements of sand wave movements. Marine Geol. 43, 49–64.

Maren, D.S., 1998. Sand waves, a state-of-the-art review and bibliography, North Sea Directorate, Ministry of Transport, Public Works and Water Management, the Netherlands, 118pp.

Németh, A.A. Modelling sand wave dynamics in shallow shelf seas, practical relevance, University of Twente, in preparation.

Soulsby, R.L., 1990. In: Le Mehaute, Bernard, Hanes, D.M. (Eds.), Ocean Engineering Science: The Sea, Vol. 9, Part A, Chapter 15: Tidal-Current Boundary Layers, pp. 523–566.

Terwindt, J.H.J., 1971. Sand waves in the southern Bight of the North Sea. Marine Geology 10, 51–67.

Tobias, C.J., 1989. Morphology of sand waves in relation to current, sediment and wave data along the Eurogeul, North Sea; Report GEOPRO 1989.01; Department of Physical Geography, University of Utrecht, The Netherlands.

Van der Molen, J., 2000. Influence of wind-driven flow on the net transport in the North Sea. In: Proceedings of the 10th International Biennial Conference On Physics of Estuaries and Coastal Seas, VIMS, pp. 285–288.

Van Rijn, L.C., 1993. Handbook of Sediment Transport by Currents and Waves. Delft Hydraulics, Delft, The Netherlands.

Whitehouse, R.J.S., Damgaard, J.S., Langhorne, D.N., 2000. Sand waves and seabed engineering: application to submarine cables. Proceedings of the Marine Sandwave Dynamics, Lille, France, pp. 227–234.